JOURNAL OF GEOPHYSICAL RESEARCH, VOL. 103, NO. C11, PAGES 24,983–24,989, OCTOBER 15, 1998

Monte Carlo simulations of the microwave emissivity of the sea surface

Quanhua Liu[1]
Alfred-Wegener-Institute for Polar and Marine Research, Bremerhaven, Germany

Clemens Simmer
Institute of Meteorology, University of Bonn, Bonn, Germany

Eberhard Ruprecht
Institute of Marine Sciences, Kiel, Germany

Abstract. A Monte Carlo model is developed to calculate the microwave emissivity of the sea surface based on the Kirchhoff approximation combined with modified Fresnel coefficients. The modified Fresnel coefficient depends on the incident angle of the electromagnetic wave and the height variance of small-scale roughness, which is an approximation to account partly for the scattering effect from small ripples. The advantage of the Monte Carlo model is its inherent capability to treat multiple scattering events. Using a two-dimensional Gaussian distribution for the sea surface slope variability, the model is capable of simulating the azimuthal dependency of the microwave emission caused by the alignment of waves perpendicular to the wind direction. Good agreement between model calculations and measurements is obtained.

1. Introduction

Accurate knowledge of reflection and emission characteristics of the ocean surface as a function of surface conditions is a prerequisite for deriving microwave retrieval algorithms [e.g., *Bauer and Schluessel*, 1993; *Karstens et al.*, 1994; *Kummerow and Giglio*, 1994] for surface and atmospheric parameters over oceanic areas. The reflection and emission characteristics of the ocean surface depend on the dielectric constant, which is a function of temperature and salinity, and on the roughness of the ocean surface. The latter is usually divided into the following three parts: roughness elements larger than the electromagnetic wavelength described by a surface element normal distribution (the so-called stationary phase approximation), subscale surface roughness, and foam [e.g., *Guissard et al.*, 1986; *Trokhimovski and Irisov*, 1995; *Wisler and Hollinger*, 1977; *Wentz*, 1975; *Wu and Fung*, 1972]. These parameters are usually estimated as functions of meteorological conditions (e.g., wind speed, stability, and temperature).

The two-scale (small irregularities superimposed on large undulations) scattering model has been well described by *Wu and Fung* [1972] and *Wentz* [1975]. The range of validity of the model for the perfect conducting random surface is discussed by *Pan and Fung* [1987].

Among the motivations for our study are to overcome difficulties that arise for large incidence angles [*Guissard et al.*, 1994] and to consider multiple scattering events by using the Monte Carlo approach. Another goal is to study three-dimensional radiative effects from clouds, together with the rough surface. In section 2 we discuss the characteristics of the sea surface in the field of remote sensing. In section 3 we describe our Monte Carlo method in detail. In section 4, comparisons are carried out between model calculations and measurements. In section 5, first results are discussed.

2. Foam and Roughness of Sea Surface

Foam is produced by the mixture of air and water and is generated by large wind speeds. The air volume fraction in the foam is about 0.95. The foam coverage may be expressed by [*Tang*, 1974]

$$d = 7.75 \times 10^{-6}(V/V_0)^{3.231} \tag{1}$$

where V is the wind speed in meters per second at 10 m above sea surface and V_0 is a constant of 1 m s^{-1}. The total reflectivity is calculated from the sum of the foam reflectivity weighted with the foam coverage d and the reflectivity of water weighted with the water coverage $(1 - d)$.

The sea surface roughness is commonly described by the roughness spectrum of the sea surface. We choose the angular-independent roughness spectrum $S(K)$ from *Bjerkaas and Riedel* [1979] and an angular function of $\cos^2 \alpha$ according to *Pierson et al.* [1955], where K is the wavenumber and α is the azimuth angle away from the upwind direction. The roughness spectrum $S(K)$ is assumed to be a function of the friction velocity of the wind only. The mean slope variance of a rough sea surface is then calculated from its roughness spectrum by

$$\sigma^2 = \frac{1}{\pi}\int_0^{\infty}\int_{-\pi}^{\pi} K^2 S(K)\, dK \cos^2 \alpha\, d\alpha \tag{2a}$$

The slope variance along the upwind and downwind direction is then given by

[1]Now at Raytheon STX, Lanham, Maryland.

Paper number 98JC01626.
0148-0227/98/98JC-01626$09.00

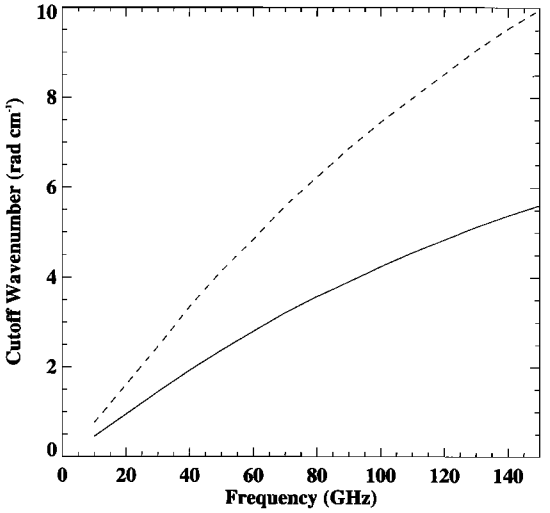

Figure 1. Variation of cutoff wavenumber K_c with frequency of the incidence electromagnetic wave. The solid line, dotted line, and dashed line are for friction velocities of 12, 50, and 80 cm s^{-1}, respectively.

$$\sigma_u^2 = \frac{1}{\pi}\int_0^{\infty}\int_{-\pi}^{\pi} K^2 S(K)\, dK \cos^2\alpha \cos^2\alpha\, d\alpha = \tfrac{3}{4}\sigma^2 \tag{2b}$$

and the slope variance along the crosswind direction is given by

$$\sigma_c^2 = \frac{1}{\pi}\int_0^{\infty}\int_{-\pi}^{\pi} K^2 S(K)\, dK \sin^2\alpha \cos^2\alpha\, d\alpha = \tfrac{1}{4}\sigma^2 \tag{2c}$$

The height variance (i.e., displacement variance) is given by

$$\zeta^2 = \frac{1}{\pi}\int_0^{\infty}\int_{-\pi}^{\pi} S(K)\cos^2\alpha\, dK\, d\alpha = \int_0^{\infty} S(K)\, dK \tag{3a}$$

As mentioned above, the foam-free sea surface roughness is usually characterized by two scales, the large-scale and the small-scale surface roughness. The large-scale surface roughness is governed by gravity force (gravity waves), while the small-scale surface roughness (capillary waves) is mainly driven by surface tension. Several criteria for separating the small-scale surface from the large-scale surface have been suggested in the literature [*Wentz*, 1975; *Ulaby et al.*, 1981]. We select the criteria from *Guissard and Sobieski* [1987] for the small scale:

$$k\zeta_R \ll 1 \tag{3b}$$

$$\frac{K_c}{k} \ll 1 \tag{3c}$$

where k ($k = 2\pi f/c$, where c is the speed of light and f is the frequency) is the wavenumber of the incident electromagnetic wave, K_c is the cutoff wavenumber separating the small-scale surface roughness from the large-scale surface roughness, and ζ_R is the height variance for small ripples. Combining (3b) and (3c) by postulating $k\zeta_R = K_c/k$, the cutoff wavenumber K_c is obtained from

$$\frac{K_c^2}{k^4} = \zeta_R^2 = \int_{K_c}^{\infty} S(K)\, dK \tag{4}$$

The low limit of the friction velocity in the surface roughness spectrum that we used here is 12 cm s^{-1}. The low limit is acceptable for the application when considering the history of waves and air-sea interactions. The friction velocity of 80 cm s^{-1} is a reasonable upper limit for (4).

Figure 1 shows that K_c increases with increasing frequency f of the electromagnetic wave and friction velocity of the wind. The behavior can also be seen from (4). For a constant friction velocity the roughness spectrum $S(K)$ is fixed. The left side of (4) decreases with an increase of the wavenumber k (equivalent to frequency f), which requires an increase of K_c to maintain (4). For a given f of the electromagnetic wave, the right side of (4) increases with friction velocity because the roughness spectrum $S(K)$ at high frequencies increases rapidly with the increase of the friction velocity, so that it requires an increase of K_c to remain the equal sign of (4). Although (4) holds, (3a)–(3c) will fail for very high wind speeds. Similar to (2a)–(2c), the surface slope variance for the large-scale surface roughness is calculated from

$$m^2 = \frac{1}{\pi}\int_0^{K_c}\int_{-\pi}^{\pi} K^2 S(K)\, dK \cos^2\alpha\, d\alpha \tag{5a}$$

The slope variance along the upwind and downwind direction is given by

$$m_u^2 = \frac{1}{\pi}\int_0^{K_c}\int_{-\pi}^{\pi} K^2 S(K)\, dK \cos^2\alpha \cos^2\alpha\, d\alpha = \tfrac{3}{4}m^2 \tag{5b}$$

and the slope variance along the crosswind direction is given by

$$m_c^2 = \frac{1}{\pi}\int_0^{K_c}\int_{-\pi}^{\pi} K^2 S(K)\, dK \sin^2\alpha \cos^2\alpha\, d\alpha = \tfrac{1}{4}m^2 \tag{5c}$$

3. Methodology

We use the Monte Carlo method to simulate stochastic processes of photons [*Liu et al.*, 1996] for single and multiple reflection events at the sea surface. As discussed in section 2, the method is to combine the limit of Kirchhoff approximation with part of the scattering effect from small-scale roughness separated by the cutoff wavenumber K_c. The small-scale surface roughness is superimposed onto the large-scale surface roughness. The emissivity of the sea surface at an observation zenith angle θ is defined by

$$\begin{bmatrix}\varepsilon_v(\theta)\\ \varepsilon_h(\theta)\end{bmatrix} = \begin{bmatrix}1\\1\end{bmatrix} - \begin{bmatrix}\Gamma_v(\theta)\\ \Gamma_h(\theta)\end{bmatrix} \tag{6}$$

where Γ is reflectivity. The subscripts v and h denote the vertical and horizontal polarization, respectively. In this paper we assume that $\theta > 90°$ is for the downward direction (from the atmosphere to the ocean). For a calm water surface the reflectivity can be described by Fresnel's law, i.e., a specular reflection model. For large-scale surface roughness the scattering is treated according to the Kirchhoff model under the stationary-phase approximation. In this approximation the large-scale surface is assumed to be a set of tangent planes or facets, in which the local reflection obeys Fresnel's law. The total reflectivity is then obtained by averaging the Fresnel reflection coefficients of the individual facets weighted with the slope probability density distribution. The commonly used Gaussian

distribution for the surface slope is adopted here. The reflectivity for the large-scale surface roughness is then written as [e.g., *Ulaby et al.*, 1981; *Tsang et al.*, 1985]

$$\begin{bmatrix}\Gamma_v(\theta)\\ \Gamma_h(\theta)\end{bmatrix} = \frac{1}{4\pi|\cos\theta|}\int_0^{2\pi}\int_0^{\pi/2}\mathbf{S}\begin{bmatrix}1\\1\end{bmatrix}\frac{q^4}{2m_u m_c q_z^4}$$

$$\cdot\exp\left[\frac{-1}{2q_z^2}\left(\frac{q_x^2}{m_u^2}+\frac{q_y^2}{m_c^2}\right)\right]\sin\theta_s\,d\theta_s\,d\phi_s \tag{7}$$

where

$$q_x = \sin\theta_s\cos\phi_s - \sin\theta\cos\phi \tag{8a}$$

$$q_y = \sin\theta_s\sin\phi_s - \sin\theta\sin\phi \tag{8b}$$

$$q_z = \cos\theta_s - \cos\theta \tag{8c}$$

$$q^2 = q_x^2 + q_y^2 + q_z^2 \tag{8d}$$

where θ, ϕ and θ_s, ϕ_s are the zenith and azimuth angles of the incident and scattering direction, respectively.

The scattering matrix S in (7) is represented by

$$\mathbf{S} = \begin{bmatrix}a|R_v(\theta_l)|^2 & b|R_h(\theta_l)|^2\\ b|R_v(\theta_l)|^2 & a|R_h(\theta_l)|^2\end{bmatrix} \tag{9}$$

where

$$a = \left|\frac{\sin\theta\cos\theta_s - \sin\theta_s\cos\theta\cos(\phi_s-\phi)}{\sin 2\theta_l}\right|^2 \tag{10a}$$

$$b = \left|\frac{\sin\theta_s\sin(\phi_s-\phi)}{\sin 2\theta_l}\right|^2 \tag{10b}$$

$$\cos 2\theta_l = -\cos\theta\cos\theta_s - \sin\theta\sin\theta_s\cos(\phi_s-\phi) \tag{10c}$$

The local Fresnel reflection coefficients for the local incident angle θ_l are

$$|R_h(\theta_l)|^2 = \left|\frac{\cos\theta_l - (\varepsilon_w - \sin^2\theta_l)^{1/2}}{\cos\theta_l + (\varepsilon_w - \sin^2\theta_l)^{1/2}}\right|^2 \tag{11a}$$

$$|R_v(\theta_l)|^2 = \left|\frac{\varepsilon_w\cos\theta_l - (\varepsilon_w - \sin^2\theta_l)^{1/2}}{\varepsilon_w\cos\theta_l + (\varepsilon_w - \sin^2\theta_l)^{1/2}}\right|^2 \tag{11b}$$

in which ε_w is the complex relative dielectric constant of water.

To simplify the Monte Carlo simulation, (7) is rewritten in the local coordinate system of the surface facet as a function of the tilting angles θ_n and ϕ_n.

$$\begin{bmatrix}\Gamma_v(\theta)\\ \Gamma_h(\theta)\end{bmatrix} = \frac{1}{4\pi|\cos\theta|}\int_0^{2\pi}\int_0^{\pi/2}\mathbf{S}\begin{bmatrix}1\\1\end{bmatrix}\frac{4\cos\theta_l\sin\theta_n}{2m_u m_c\cos^4\theta_n}$$

$$\cdot\exp\left[\frac{-\tan^2\theta_n}{2}\left(\frac{\cos^2\phi_n}{m_u^2}+\frac{\sin^2\phi_n}{m_c^2}\right)\right]d\theta_n\,d\phi_n \tag{12}$$

With the definitions

$$dR_1 = \frac{d\phi_n}{2\pi} \tag{13a}$$

$$dR_2 = \left(\frac{\cos^2\phi_n}{m_u^2}+\frac{\sin^2\phi_n}{m_c^2}\right)$$

$$\cdot\exp\left[\frac{-\tan^2\theta_n}{2}\left(\frac{\cos^2\phi_n}{m_u^2}+\frac{\sin^2\phi_n}{m_c^2}\right)\right]\frac{\sin\theta_n}{\cos^3\theta_n}d\theta_n \tag{13b}$$

we can write

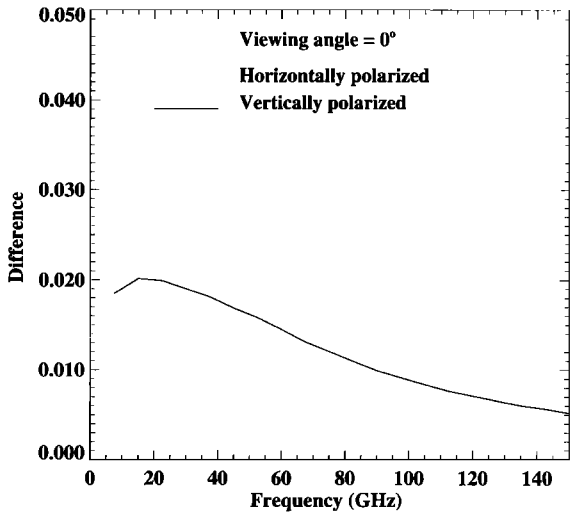

Figure 2. Differences between the original and modified Fresnel reflection coefficient for a friction velocity of 50 cm s^{-1} and a sea surface temperature of 291 K for vertical (solid line) and horizontal (dashed line) polarization. The viewing direction is from nadir.

$$\begin{bmatrix}\Gamma_v(\theta)\\ \Gamma_h(\theta)\end{bmatrix} = \frac{1}{|\cos\theta|}$$

$$\cdot\int_0^1\int_0^1\mathbf{S}\begin{bmatrix}1\\1\end{bmatrix}\frac{m_u m_c\cos\theta_l}{(m_c^2\cos^2\phi_n + m_u^2\sin^2\phi_n)\cos\theta_n}dR_1\,dR_2 \tag{14}$$

with

$$\phi_n = 2\pi R_1 \tag{15a}$$

$$\tan^2\theta_n = -\frac{2m_u^2 m_c^2}{m_u^2\sin^2\phi_n + m_c^2\cos^2\phi_n}\ln(1-R_2) \tag{15b}$$

Therefore two random numbers R_1 and R_2 describe the statistics of the tilting angles θ_n and ϕ_n. Once ϕ_n and then θ_n are determined from R_1 and R_2, the local incident angle θ_l and the scattering direction can be calculated as follows:

$$\cos\theta_l = -\cos\theta\cos\theta_n + \sin\theta\sin\theta_n\cos(\phi-\phi_n) \tag{15c}$$

$$\sin\theta_s\cos\phi_s = \sin\theta\cos\phi + \cos\theta\sin 2\theta_n\cos\phi_n - 2\sin\theta\sin^2\theta_n\cos\phi_n\cos(\phi-\phi_n) \tag{15d}$$

$$\sin\theta_s\sin\phi_s = \sin\theta\sin\phi + \cos\theta\sin 2\theta_n\sin\phi_n - 2\sin\theta\sin^2\theta_n\sin\phi_n\cos(\phi-\phi_n) \tag{15e}$$

$$\cos\theta_s = \sin\theta\sin 2\theta_n\cos(\phi-\phi_n) - \cos\theta\cos 2\theta_n \tag{15f}$$

The reflected part of the photon is then written as

$$\begin{bmatrix}\gamma_v\\ \gamma_h\end{bmatrix} = \frac{c}{|\cos\theta|}\mathbf{S}\begin{bmatrix}1\\1\end{bmatrix} \tag{15g}$$

with

$$c = \frac{m_u m_c\cos\theta_l}{(m_u^2\sin^2\phi_n + m_c^2\cos^2\phi_n)\cos\theta_n} \tag{15h}$$

If $\theta_s > 90°$, the photon is assumed to undertake another

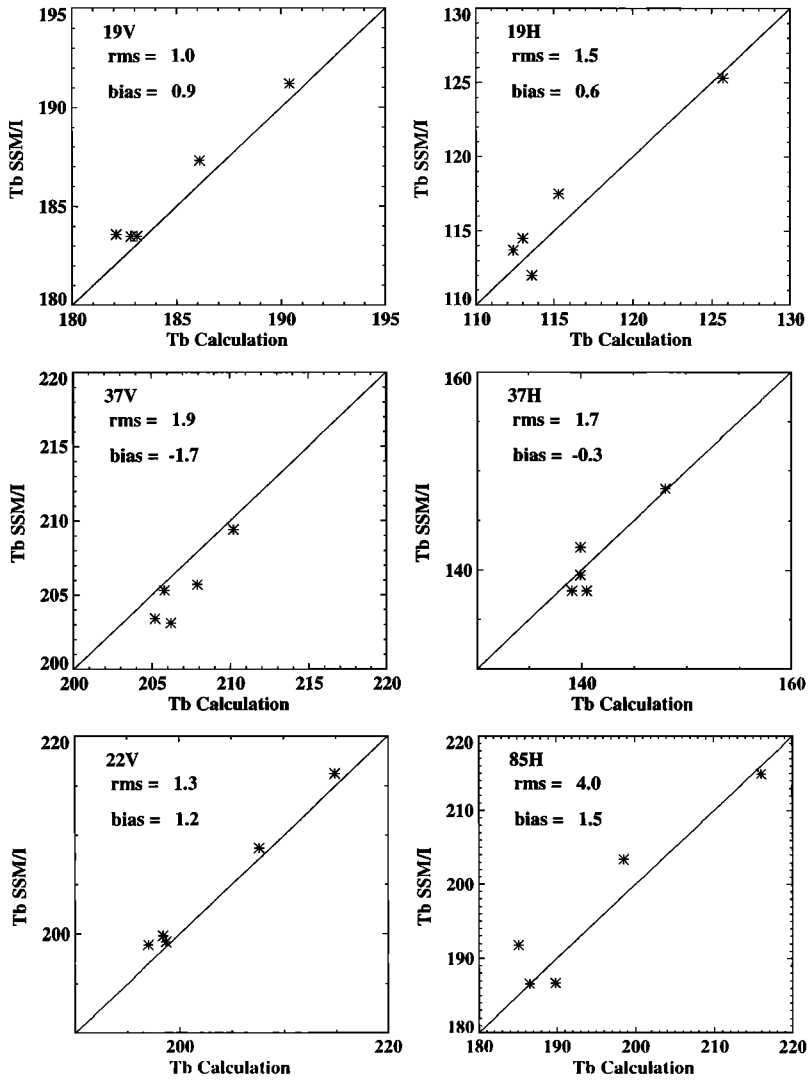

Figure 3. Comparison of brightness temperatures T_b at a zenith angle of 53° between model calculations and special sensor microwave/imager (SSM/I) measurements during the International Cirrus Experiment on the North Sea in October 1989.

reflection event (i.e., multiple scattering events) with the water surface. The reflection part for the photon after k reflection events can be expressed as

$$\begin{bmatrix} \gamma_v \\ \gamma_h \end{bmatrix} = \frac{1}{|\cos\theta|} c_k \mathbf{S}_k c_{k-1}\mathbf{S}_{k-1} \cdots c_1 \mathbf{S}_1 \begin{bmatrix} 1 \\ 1 \end{bmatrix} \tag{16}$$

Where c_i (see (15h)) and $\mathbf{S}_i$ (see (9)) depend on the incoming and outgoing directions of the ith reflection event. Upward directed photons (i.e., $\theta_s < 90°$) can also take another reflection event with the surface, but the possibility of this should be small. This case is not considered in the present model owing to the limit imposed by the representation of the ocean surface elements by a surface normal distribution. The same circumstances prohibit the exact inclusion of shadowing. Another assumption is that the distribution of $S(k)$ remains the same for all scattering processes, which is not exactly true.

The electromagnetic wave can be reflected and diffracted by small ripples before and after the reflection from the background large-scale facets. Comprehensive treatments of the scattering effects from small ripples can be found in the literature [e.g., *Wu and Fung*, 1972; *Wentz*, 1975]. We use a simple approximation (modified Fresnel coefficient) to account partly for the scattering effects. We follow *Guissard and Sobieski* [1987] by using

$$|R_v|^2 = |R_v|^2 \exp(-4k^2\zeta_R^2 \cos^2\theta_i) \tag{17a}$$

$$|R_h|^2 = |R_h|^2 \exp(-4k^2\zeta_R^2 \cos^2\theta_i) \tag{17b}$$

Differences between the original and the modified Fresnel reflection coefficients reach a maximum at about 20 GHz, then decrease with frequency (Figure 2). Both k and ζ_R are the function of frequency. For large wind speeds, foam has to be taken into account. The complex relative dielectric constant of foam can be parametrized according to *Droppleman* [1970]

$$\varepsilon_f = \varepsilon_w \left[1 - \frac{3V_a(\varepsilon_w - 1)}{(2\varepsilon_w + 1) + V_a(\varepsilon_w - 1)} \right] \tag{18}$$

where V_a is the air volume fraction in foam, assumed to be between 0.94 and 0.99. The reflectivity of foam depends also

on the thickness of the foam layer [e.g., *Schrader and Liu*, 1995]. *Stogryn* [1972] derived an analytical expression for foam emissivity from measurements that was between 13.4 and 37 GHz. In this paper the reflectivity of the foam is calculated as a function of sea surface temperature, frequency, and surface wind speed, following *Ulaby et al.* [1986].

The microwave reflectivity of the sea surface can now be calculated from the Monte Carlo model by sending many photons (e.g., 10,000) from the detector direction (θ, ϕ) to the sea surface. Using (11a), (11b), (15a)–(15h), and (16) we can calculate the reflection part for each photon. The reflectivity of the sea surface is then carried out by averaging the reflected parts of the photons.

4. Comparisons With Measurements

In order to test our algorithm, we performed two calculations, first with measurements at the North Sea and second with data given by *Hollinger* [1970]. Simultaneous measurements from the special sensor microwave/imager (SSM/I) and radiosonde and ship synoptic observations for clear sky cases were collected during the International Cirrus Experiment in October 1989. The ship measurements were performed from the German research vessel POSEIDON cruising on the North Sea. The time differences between satellite measurements and radiosonde and ship measurements were less than 15 min. The observed atmospheric parameters were used as input for our radiative transfer code [*Liu and Ruprecht*, 1996]. The calculated brightness temperatures agree, in general, with the satellite measurements (Figure 3). The rms error between the modeled and measured microwave brightness temperature T_b is less than 2 K for 19.35, 22.235, and 37 GHz. The rms error reaches 4 K for the horizontally polarized T_b at 85.5 GHz. We do not compare the vertically polarized component of the brightness temperature T_b at 85.5 GHz because this channel

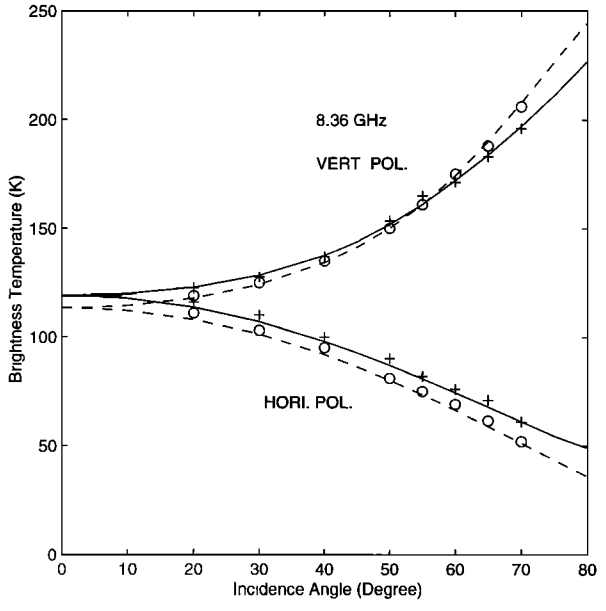

Figure 4a. Comparisons between model calculations (dashed line for 3.5 m s^{-1}, solid line for 13.5 m s^{-1}) and the surface measured brightness temperatures (circles for 0.5 m s^{-1}, crosses for 13.5 m s^{-1}) at 8.36 GHz by *Hollinger* [1970] for different incident angles.

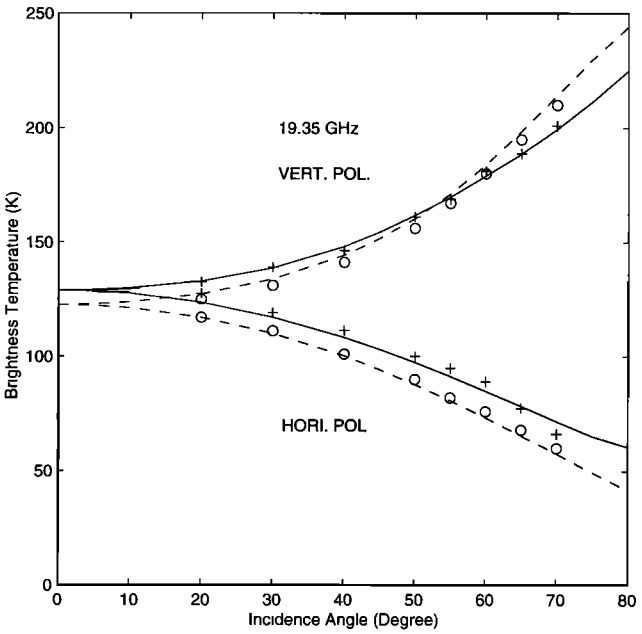

Figure 4b. Same as Figure 4a, but for 19.35 GHz.

was not functioning at that time. Another comparison was performed with the surface measurements taken from *Hollinger* [1970]. The surface measurements are at 8.36 and 19.35 GHz for a sea surface temperature of 291 K and wind speeds of 0.5 and 13.5 m s^{-1} measured at 43 m above the sea surface. The errors of the measurements estimated by *Hollinger* [1970] are between 5% and 10%. Effects due to foam and the reflected atmospheric radiation were removed. The model calculations were carried out for the same frequencies and surface temperatures, but with wind speeds of 3.5 and 13.5 m s^{-1}. A wind speed of 3.5 m s^{-1} instead of 0.5 m s^{-1} was applied in the calculations because 3.5 m s^{-1} corresponds to the minimum friction velocity of 12 cm s^{-1} in the sea surface roughness spectrum of *Bjerkaas and Riedel* [1979]. The model calculations were performed by setting $m_u = m_c$ in (12) because the relative azimuth angle of the measurement of *Hollinger* [1970] is not known. For $m_u = m_c$ a difference of a constant factor of 2 is found in the exponential expressions given by *Ulaby et al.* [1986], equation (18.33)] and *Wu and Fung* [1972, equation (32)]. Better agreement with *Hollinger*'s [1970] measurements is achieved with the exponential expression by *Wu and Fung* [1972] (Figures 4a and 4b). The rms error between the modeled and measured T_b is 4.2 K for 8.36 GHz and 5.5 K for 19.35 GHz.

5. Sensitivity Calculations

Further calculations were conducted to show the applicability of the present method. The dependency of brightness temperature on azimuth angle of the viewing angle influences the retrieval of the sea surface wind from SSM/I measurements [*Wentz*, 1992]. We performed calculations to quantify the effect of azimuth angle variations on the upwelling T_b at the sea surface (Figure 5). The vertically polarized T_b reaches a maximum in the upwind-downward directions and a minimum in the crosswind direction. Opposite results are found for the horizontally polarized T_b. These behaviors are similar to the measurements by *Wentz* [1992] and *Yueh et al.* [1995].

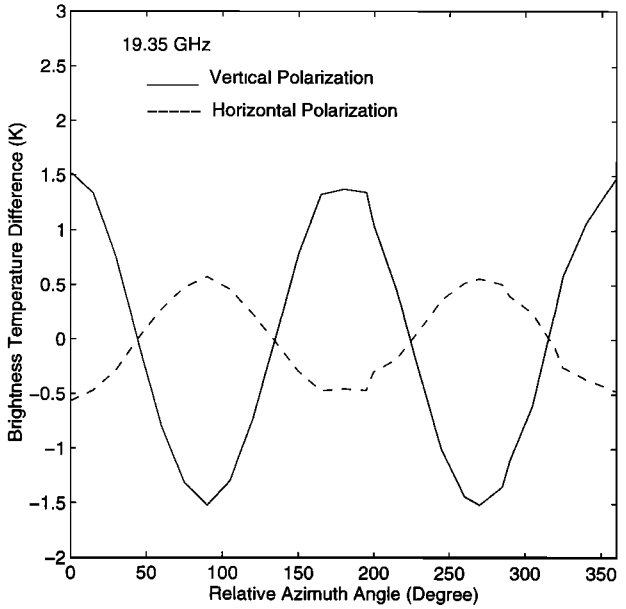

Figure 5. Difference between the modeled T_b at 19.35 GHz and its mean value averaged over all azimuth angles.

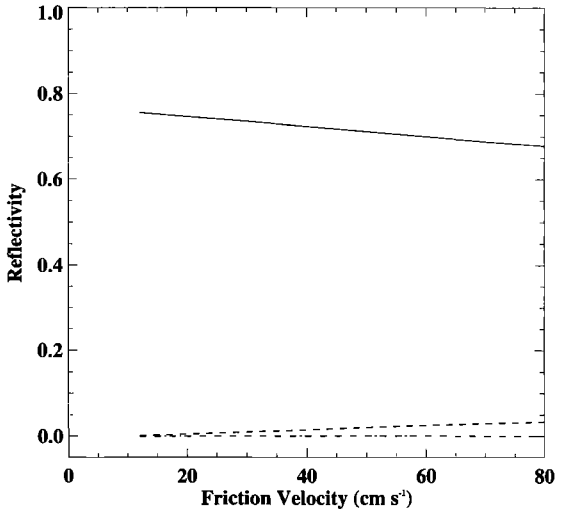

Figure 7. Contribution of single and multiple reflection events to the total reflectivity at 19.35 GHz as a function of friction velocity. The zenith angle is 60°. The solid and dotted lines are the horizontal and vertical reflectivities from single scattering events, respectively. The dashed line is the horizontal reflectivity from multiple scattering events. The dot-dashed line is the vertical reflectivity from multiple scattering events.

Multiple scatterings of photons at the sea surface can affect the total reflectivity. The percentage of photons that have undertaken two or more reflection events increases dramatically with the friction velocity of wind and the incidence angle of the electromagnetic wave (Figure 6). The percentage is less than 1% at nadir, but it increases to 20% at a viewing angle of 60° for a friction velocity of 150 cm s^{-1}. The effects of single and multiple reflections on the microwave reflectivity of sea surface are shown in Figure 7, in which calculations were made at 19.35 GHz for a zenith angle of 60° and a sea surface temperature of 291 K. The total reflectivity is the sum from

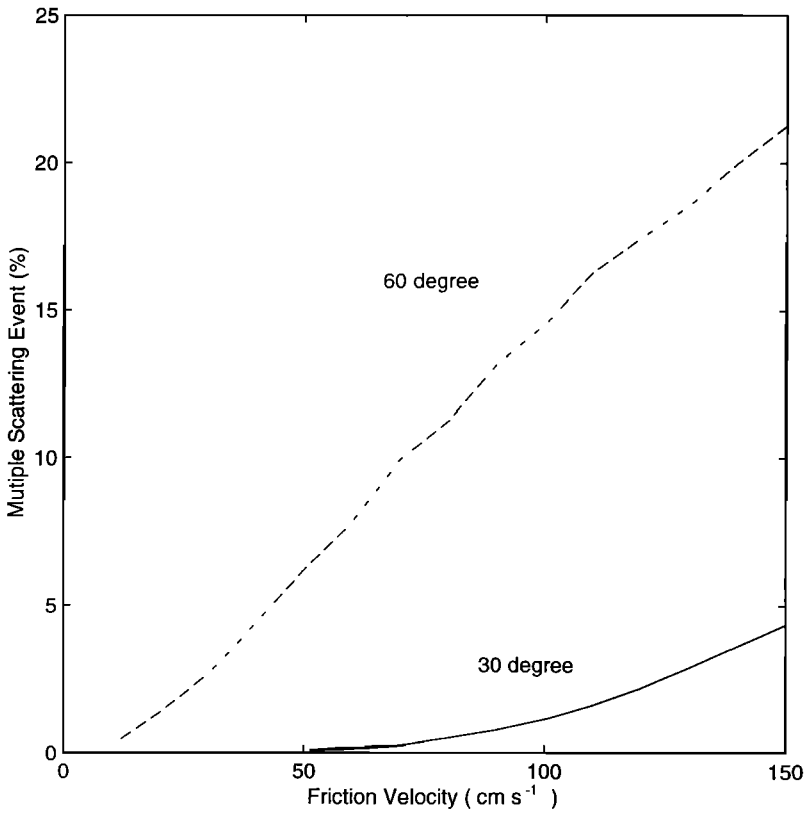

Figure 6. Percentage of photons that have undertaken two or more reflection events as a function of friction velocity for zenith angles of 30° (solid line) and 60° (dashed line).

single and multiple reflections. Obviously, the contribution of multiple reflection to the vertically polarized component of the total reflectivity is small. However, the contribution of multiple reflections to the horizontally polarized component can reach almost 10% (Figure 7).

As mentioned in section 1, difficulties arise in numerical calculations from using (7) directly because the integrand is almost a delta function for large incidence angles and a near specular reflection direction. Such problems can be avoided by using the Monte Carlo method because we simulate individual photons instead of using the delta function explicitly. Model results for large angles seem reasonable, and negative emissivities do not appear.

6. Discussion

Although agreement between measurements and model calculations is achieved, some problems, such as the sea roughness spectrum and the criteria for the cutoff wavenumber, need to be studied further. Only part of the scattering effect from small ripples is considered with the modified Fresnel coefficient. The application of the present model is limited for calculating signatures of the passive microwave measurements such as SSM/I. The absolute error of the model calculation is estimated to be less than 3%. Since the model is a noncoherent one, it cannot correctly treat a perfectly conducting rough surface and anomalous microwave radiative temperatures over the ice surface, i.e., larger horizontally than vertically polarized microwave radiative temperatures. A more physical model [e.g., *Wentz*, 1975] is required to account for the diffractions of the electromagnetic wave from small ripples. Different choices for the roughness spectrum and the criteria for the cutoff wavenumber can slightly change the simulated surface emissivity. In addition, the microwave emissivity of the sea surface, which is calculated from the Gaussian slope distribution, is upwind-downwind symmetric. This symmetry conflicts with the upwind-downwind asymmetry in the scatterometer response [e.g., *Sobieski et al.*, 1991]. However, the only way to incorporate these effects, to correctly include shadowing, and to completely describe multiple scattering is the replacement of the slope distribution model by a complete ocean surface topography.

References

Bauer, P., and P. Schluessel, Rainfall, total water, ice water, and water vapor over sea from polarized microwave simulations and special sensor microwave/imager data, *J. Geophys. Res.*, *98*, 20,737–20,759, 1993.

Bjerkaas, A. W., and F. P. Riedel, Proposed model for the elevation spectrum of a wind-roughened sea surface, *Tech. Memo. JHUIAPL TG 1328*, 31 pp., Appl. Phys. Lab., Johns Hopkins Univ., Laurel, Md., 1979.

Droppleman, J. D., Apparent microwave emissivity of sea foam, *J. Geophys. Res.*, *75*, 696–698, 1970.

Guissard, A., and P. Sobieski, An approximate model for the microwave brightness temperature of the sea, *Int. J. Remote Sens.*, *8*, 1607–1627, 1987.

Guissard, A., C. Baufays, and P. Sobieski, Sea surface description requirements for electromagnetic scattering calculations, *J. Geophys. Res.*, *91*, 2477–2492, 1986.

Guissard, A., P. Sobieski, and A. Laloux, Radiative transfer equation with surface scattering for ocean and atmospheric parameters retrieval from radiometric measurements, *Int. J. Remote Sens.*, *15*, 1743–1760, 1994.

Hollinger, J. P., Passive microwave measurements of sea surface, *J. Geophys. Res.*, *75*, 5209–5213, 1970.

Karstens, U., C. Simmer, and E. Ruprecht, Remote sensing of cloud liquid water, *Meteorol. Atmos. Phys.*, *54*, 157–171, 1994.

Kummerow, C., and L. Giglio, A passive microwave technique for estimating rainfall and vertical structure information from space, I, Algorithm description, *J. Appl. Meteorol.*, *33*, 3–18, 1994.

Liu, Q., and E. Ruprecht, A radiative transfer model: Matrix operator method, *Appl. Opt.*, *35*, 4229–4237, 1996.

Liu, Q., C. Simmer, and E. Ruprecht, Three-dimensional radiative transfer effects of clouds in the microwave spectral range, *J. Geophys. Res.*, *101*, 4289–4298, 1996.

Pan, G. W., and A. K. Fung, A scattering model for perfect conducting random surface, II, Range of validity, *Int. J. Remote Sens.*, *8*, 1595–1605, 1987.

Pierson, W. J., G. Neumann, and R. W. James, Practical methods for observing and forcasting ocean waves by means of wave spectra and statistics, *Publ. 603*, Hydrogr. Off., U. S. Navy, Washington, D. C., 1955.

Schrader, M., and Q. Liu, On the use of different ocean surface models in radiative transfer calculation in *Microwave Radiometry and Remote Sensing of the Environment*, edited by D. Solimini, pp. 209–217, VSP, Utrecht, Netherlands, 1995.

Sobieski, P., A. Guissard, and C. Braufays, Synergic inversion technique for active and passive microwave remote sensing of the ocean, *IEEE. Trans. Geosci. Remote Sens.*, *29*, 391–406, 1991.

Stogryn, A., The emissivity of sea foam at microwave frequencies, *J. Geophys. Res.*, *77*, 1658–1666, 1972.

Tang, C. C. H., The effect of droplets in the air-sea transition zone on the sea brightness temperature, *J. Phys. Oceanogr.*, *4*, 579–593, 1974.

Trokhimovski, Y. G., and V. G. Irisov, Wind speed and direction measurement using microwave polarimetric radiometers, *Tech. Memo. ERL ETL-250*, 35 pp., Natl. Oceanic and Atmos. Admin., Silver Spring, Md., 1995.

Tsang, L., J. A. Kong, and R. T. Shin, *Theory of Microwave Remote Sensing*, 613 pp., Wiley-Intersci., New York, 1985.

Ulaby, F., R. Moore, and A. Fung, *Microwave Remote Sensing, Active and Passive*, vol. 1, *Fundamentals and Radiometry*, 456 pp., Addison-Wesley, Reading, Mass., 1981.

Ulaby, F., R. Moore, and A. Fung, *Microwave Remote Sensing, Active and Passive*, vol. 3, *From Theory to Application*, pp. 1065–2162, Addison-Wesley, Reading, Mass., 1986.

Wentz, F. J., A two-scale scattering model for foam-free sea microwave brightness temperature, *J. Geophys. Res.*, *80*, 3441–3446, 1975.

Wentz, F. J., Measurement of oceanic wind vector using satellite microwave radiometers, *IEEE Trans. Geosci. Remote Sens.*, *30*, 960–972, 1992.

Wisler, M. M., and J. P. Hollinger, Estimation of marine environmental parameters using microwave radiometric remote sensing systems, *NRL Memo. Rep.*, *3661*, 27 pp., Nav. Res. Lab., Washington, D. C., 1977.

Wu, S. T., and A. K. Fung, A noncoherent model for microwave emissions and backscattering from the sea surface, *J. Geophys. Res.*, *77*, 5917–5929, 1972.

Yueh, S. H., W. J. Wilson, F. K. Li, S. V. Nghiem, and W. B. Ricketts, Polarimetric measurements of sea surface brightness temperatures using an aircraft K-band radiometer, *IEEE Trans. Geosci. Remote Sens.*, *33*, 85–92, 1995.

Q. Liu, Raytheon STX, 4400 Forbes Boulevard, Lanham, MD 20706. (e-mail: qliu@ccmail.stx.com)

E. Ruprecht, Institute of Marine Sciences, Düsternbrooker Weg 20, 24105 Kiel, Germany.

C. Simmer, Institute of Meteorology, University of Bonn, Auf dem Hügel 20, 53121 Bonn, Germany.

(Received August 29, 1996; revised September 12, 1997; accepted October 15, 1997.)